Available online at www.sciencedirect.com
SCIENCE DIRECT®
J. Chem. Thermodynamics 36 (2004) 609–618
JCT
www.elsevier.com/locate/jct

# The low-temperature heat capacity of some lanthanide zirconates

S. Lutique [a,1], P. Javorskỳ [a,2], R.J.M. Konings [a,*], J.-C. Krupa [b], A.C.G. van Genderen [c], J.C. van Miltenburg [c], F. Wastin [a]

[a] European Commission, Joint Research Center, Institute for Transuranium Elements, P.O. Box 2340, 76125 Karlsruhe, Germany
[b] Institut de Physique Nucléaire, CNRS-IN2P3, 91406 Orsay Cedex, France
[c] Chemical Thermodynamics Group, Utrecht University, Padualaan 8, 3584 CH, Utrecht, Netherlands

Received 29 January 2004; accepted 29 March 2004
Available online 8 May 2004

**Abstract**

The heat capacities of the lanthanide zirconates $Gd_2Zr_2O_7$ and $Eu_2Zr_2O_7$ with pyrochlore structure were measured by adiabatic calorimetry and the hybrid adiabatic relaxation method in the temperature range (0.3 to 400) K. A thermal anomaly was observed for $Gd_2Zr_2O_7$ below $T = 15$ K. From the measurements the thermodynamic functions of $Gd_2Zr_2O_7$ and $Eu_2Zr_2O_7$ were determined. By combining our results with the heat capacity data of $La_2Zr_2O_7$, the lattice component of the heat capacity and the entropy were derived for the lanthanide series $Ln_2Zr_2O_7$ (Ln = La to Gd). The Schottky contributions were derived for $Ce_2Zr_2O_7$, $Nd_2Zr_2O_7$ and $Eu_2Zr_2O_7$ by subtracting the lattice component from the experimental data, and compared to the values calculated from the crystal field energy levels.


*Keywords:* Heat capacity; Pyrochlore; Calorimetry

## 1. Introduction

Pyrochlore-type compounds with general formula $A_2B_2O_7$, and especially zirconates (B = Zr), are materials with high scientific and technological importance. Recently, they have attracted attention in the scientific world as geometrically frustrated magnetic systems, exhibiting 'spin ice' behaviour [1–3]. During the last decades they have found many interesting industrial applications: they are studied for thermal barrier coating [4–7], sub-catalysts for automotive exhaust gases ($Ce_2Zr_2O_{7+y}$) [8–11] as well as for nuclear applications [12–21]. For the latter, which is the topic of our research, it is important that the chemical configuration of the lanthanide zirconate pyrochlores enables incorporation of actinides in the crystal lattice. This makes them potential candidates as inert matrix for the transmutation of actinides or as waste form for their storage.

Knowledge of the thermodynamic stability of these compounds is necessary for all industrial applications in order to determine their durability under typical process conditions. Until now only few thermodynamic studies have been reported for lanthanide zirconate pyrochlore compounds. The molar enthalpy of formation of some lanthanide zirconates $Ln_2Zr_2O_7$ were reported for Ln = La, Pr, Nd and Sm by Korneev *et al.* [22], for Ln = La by Bolech *et al.* [23–25] and for Ln = Gd by Helean *et al.* [26]. The heat capacity of some lanthanide zirconate was reported by Bolech *et al.* [24,25] (Ln = La and Ce) in the temperature range (5 to 900) K and Lutique *et al.* [16,27,28] (Ln = Nd) in the temperature range (0.4 to 1600) K. In the present study, we extend the heat capacity data with $Gd_2Zr_2O_7$ and $Eu_2Zr_2O_7$, the results of which enable us to determine the lattice and excess components in the series Ln = La to Gd.

* Corresponding author. Fax: +49-7247-951-591.
*E-mail address:* konings@itu.fzk.de (R.J.M. Konings).
[1] Current address: Commissariat à l'Energie Atomique, Centre de Cadarache, DEN/DEC/SPUA/LTEC, 13108 St. Paul lez Durance, France.
[2] Permanent address: Department of Electronic Structures, Charles University, Ke Karlovu, 12116 Prague, Czech Republic.

0021-9614/$ - see front matter © 2004 Elsevier Ltd. All rights reserved.
doi:10.1016/j.jct.2004.03.017

TABLE 1
Experimental heat capacity $C^{\circ}_{p,m}$ for $Gd_2Zr_2O_7$ obtained with the adiabatic calorimeter at temperature $T$

| $T$/K | $C^{\circ}_{p,m}$ | $T$/K | $C^{\circ}_{p,m}$ | $T$/K | $C^{\circ}_{p,m}$ | $T$/K | $C^{\circ}_{p,m}$ |
|---|---|---|---|---|---|---|---|
| | $(J \cdot K^{-1} \cdot mol^{-1})$ | | $(J \cdot K^{-1} \cdot mol^{-1})$ | | $(J \cdot K^{-1} \cdot mol^{-1})$ | | $(J \cdot K^{-1} \cdot mol^{-1})$ |
| | | | | *Run 1* | | | |
| 299.59 | 221.9 | 326.46 | 230.9 | 353.30 | 238.6 | 380.24 | 245.3 |
| 302.61 | 222.9 | 329.45 | 231.7 | 356.29 | 239.4 | 383.24 | 246.0 |
| 305.58 | 223.9 | 332.43 | 232.7 | 359.28 | 240.1 | 386.24 | 246.6 |
| 308.56 | 225.1 | 335.41 | 233.6 | 362.27 | 240.8 | 389.24 | 247.3 |
| 311.54 | 226.1 | 338.38 | 234.4 | 365.26 | 241.7 | 392.24 | 247.8 |
| 314.52 | 227.1 | 341.37 | 235.3 | 368.26 | 242.3 | 395.35 | 248.4 |
| 317.51 | 228.1 | 344.35 | 236.2 | 371.25 | 243.1 | 398.26 | 249.1 |
| 320.49 | 229.0 | 347.33 | 237.0 | 374.24 | 243.9 | 401.27 | 249.9 |
| 323.48 | 229.9 | 350.32 | 237.8 | 377.24 | 244.6 | 404.28 | 250.4 |
| | | | | *Run 2* | | | |
| 99.99 | 90.29 | 136.59 | 127.7 | 174.64 | 159.9 | 213.00 | 185.4 |
| 101.94 | 92.84 | 139.50 | 130.4 | 177.58 | 162.1 | 215.96 | 187.0 |
| 104.84 | 95.74 | 142.42 | 133.1 | 180.52 | 164.3 | 218.92 | 188.5 |
| 107.71 | 99.12 | 145.33 | 135.8 | 183.47 | 166.4 | 221.88 | 190.2 |
| 110.58 | 102.0 | 148.25 | 138.4 | 186.41 | 168.5 | 224.84 | 191.8 |
| 113.46 | 105.0 | 151.18 | 140.9 | 189.36 | 170.6 | 227.80 | 193.4 |
| 116.33 | 107.8 | 154.11 | 143.4 | 192.31 | 172.7 | 230.77 | 194.9 |
| 119.22 | 110.5 | 157.03 | 145.8 | 195.26 | 174.7 | 233.73 | 196.4 |
| 122.10 | 113.4 | 159.96 | 148.3 | 198.21 | 176.7 | 236.70 | 197.9 |
| 125.00 | 116.6 | 162.89 | 150.6 | 201.17 | 178.5 | 239.67 | 199.4 |
| 127.89 | 119.4 | 165.82 | 153.0 | 204.12 | 180.4 | 242.63 | 200.8 |
| 130.78 | 122.3 | 168.76 | 155.4 | 207.08 | 182.2 | 245.60 | 202.1 |
| 133.69 | 125.0 | 171.69 | 157.6 | 210.04 | 183.8 | 248.57 | 203.6 |
| | | | | *Run 3* | | | |
| 255.64 | 206.1 | 267.53 | 211.4 | 279.42 | 216.1 | 288.36 | 219.3 |
| 258.62 | 207.6 | 270.50 | 212.6 | 282.40 | 217.2 | 291.34 | 220.2 |
| 261.60 | 208.9 | 273.47 | 213.8 | 285.38 | 218.3 | 294.32 | 220.8 |
| 264.56 | 210.1 | 276.45 | 215.0 | | | | |
| | | | | *Run 4* | | | |
| 298.71 | 220.9 | 327.34 | 230.5 | 357.18 | 239.0 | 387.12 | 246.2 |
| 300.49 | 221.6 | 330.32 | 231.4 | 360.17 | 239.7 | 390.13 | 246.7 |
| 303.49 | 222.4 | 333.30 | 232.3 | 363.16 | 240.5 | 393.14 | 247.2 |
| 306.48 | 223.5 | 336.29 | 233.1 | 366.15 | 241.2 | 396.14 | 247.8 |
| 309.46 | 224.6 | 339.27 | 234.0 | 369.14 | 242.0 | 399.15 | 248.5 |
| 312.44 | 225.6 | 342.25 | 234.8 | 372.13 | 242.6 | 402.16 | 249.0 |
| 315.42 | 226.6 | 345.23 | 235.7 | 375.12 | 243.5 | 405.18 | 249.7 |
| 318.40 | 227.6 | 348.22 | 236.6 | 378.12 | 244.1 | | |
| 321.38 | 228.6 | 351.21 | 237.4 | 381.12 | 244.8 | | |
| 324.36 | 229.6 | 354.19 | 238.1 | 384.12 | 245.4 | | |
| | | | | *Run 5* | | | |
| 5.02 | 4.762 | 6.66 | 3.576 | 7.27 | 3.201 | 8.15 | 4.021 |
| 5.39 | 4.085 | 6.69 | 3.439 | 7.78 | 3.179 | | |
| | | | | *Run 6* | | | |
| 5.75 | 4.144 | 16.10 | 2.529 | 21.67 | 5.071 | 25.75 | 8.184 |
| 8.61 | 2.534 | 17.67 | 3.056 | 23.02 | 5.773 | 27.16 | 9.130 |
| 11.57 | 2.026 | 19.00 | 3.599 | 24.36 | 6.997 | 28.60 | 10.54 |
| | | | | *Run 7* | | | |
| 5.15 | 4.003 | 13.82 | 2.004 | 19.81 | 3.798 | 25.48 | 7.856 |
| 6.88 | 3.124 | 15.47 | 2.281 | 21.25 | 4.715 | | |
| 9.34 | 2.281 | 16.94 | 3.015 | 22.65 | 5.561 | | |
| 11.78 | 1.875 | 18.37 | 3.309 | 24.06 | 6.716 | | |
| | | | | *Run 8* | | | |
| 27.34 | 8.888 | 41.73 | 23.57 | 57.60 | 42.08 | 74.32 | 61.44 |
| 28.59 | 10.17 | 43.44 | 25.54 | 59.42 | 44.18 | 76.21 | 63.60 |
| 30.28 | 11.70 | 45.16 | 27.54 | 61.25 | 46.31 | 78.11 | 65.77 |
| 31.85 | 13.20 | 46.90 | 29.50 | 63.10 | 48.49 | 80.01 | 67.99 |

TABLE 1 (*continued*)

| $T$/K | $C^\circ_{p,m}$ | $T$/K | $C^\circ_{p,m}$ | $T$/K | $C^\circ_{p,m}$ | $T$/K | $C^\circ_{p,m}$ |
|---|---|---|---|---|---|---|---|
| | $(J \cdot K^{-1} \cdot mol^{-1})$ | | $(J \cdot K^{-1} \cdot mol^{-1})$ | | $(J \cdot K^{-1} \cdot mol^{-1})$ | | $(J \cdot K^{-1} \cdot mol^{-1})$ |
| 33.42 | 14.96 | 48.65 | 31.63 | 64.95 | 50.64 | 81.92 | 70.16 |
| 35.03 | 16.67 | 50.41 | 33.67 | 66.81 | 52.75 | 83.83 | 72.04 |
| 36.66 | 18.43 | 52.19 | 35.74 | 68.68 | 54.94 | 85.75 | 74.43 |
| 38.33 | 19.78 | 53.98 | 37.79 | 70.55 | 57.09 | 87.67 | 76.62 |
| 40.03 | 21.65 | 55.79 | 39.92 | 72.43 | 59.27 | 89.59 | 78.86 |
| | | | | *Run 9* | | | |
| 5.39 | 5.557 | 9.23 | 2.338 | 12.38 | 1.905 | 14.47 | 2.146 |
| 6.39 | 3.337 | | | | | | |
| | | | | *Run 10* | | | |
| 6.57 | 4.653 | 10.62 | 1.859 | 14.41 | 2.054 | 17.71 | 2.843 |
| 7.09 | 1.869 | 11.91 | 1.932 | 15.56 | 2.548 | 18.74 | 3.372 |
| 8.75 | 2.305 | 13.18 | 2.063 | 16.65 | 2.604 | 19.70 | 3.988 |
| | | | | *Run 11* | | | |
| 21.15 | 4.222 | 34.71 | 16.30 | 51.01 | 34.30 | 68.78 | 55.04 |
| 22.44 | 5.562 | 36.63 | 18.41 | 53.16 | 36.84 | 71.07 | 57.68 |
| 23.86 | 6.517 | 38.60 | 20.08 | 55.33 | 39.42 | 73.38 | 60.34 |
| 25.61 | 7.937 | 40.62 | 22.35 | 57.53 | 41.95 | 75.70 | 62.97 |
| 27.35 | 9.282 | 42.65 | 24.76 | 59.74 | 44.49 | 78.02 | 65.59 |
| 29.15 | 10.86 | 44.69 | 27.04 | 61.98 | 47.15 | 80.36 | 68.33 |
| 30.99 | 12.58 | 46.77 | 29.41 | 64.23 | 49.75 | | |
| 32.83 | 14.42 | 48.88 | 31.86 | 66.50 | 52.35 | | |
| | | | | *Run 12* | | | |
| 84.26 | 73.08 | 127.42 | 118.9 | 171.42 | 157.6 | 215.77 | 187.1 |
| 86.68 | 75.97 | 129.86 | 121.3 | 173.88 | 159.3 | 218.24 | 187.9 |
| 89.04 | 78.05 | 132.29 | 123.7 | 176.34 | 161.2 | 220.70 | 189.4 |
| 91.40 | 80.73 | 134.72 | 125.9 | 178.80 | 163.0 | 223.17 | 190.4 |
| 93.76 | 83.52 | 137.16 | 128.2 | 181.26 | 164.8 | 225.64 | 192.2 |
| 96.13 | 85.94 | 139.59 | 130.2 | 183.72 | 166.4 | 228.11 | 193.4 |
| 98.51 | 88.81 | 142.03 | 132.8 | 186.18 | 168.2 | 230.58 | 194.8 |
| 100.90 | 91.06 | 144.47 | 134.8 | 188.64 | 169.8 | 233.05 | 195.7 |
| 103.28 | 93.88 | 146.91 | 136.9 | 191.10 | 171.8 | 235.53 | 197.1 |
| 105.68 | 96.49 | 149.35 | 139.3 | 193.56 | 173.3 | 238.00 | 198.4 |
| 108.08 | 99.44 | 151.80 | 141.2 | 196.03 | 175.1 | 240.47 | 199.4 |
| 110.48 | 101.8 | 154.25 | 143.3 | 198.49 | 176.5 | 242.94 | 200.6 |
| 112.89 | 104.4 | 156.70 | 145.3 | 200.95 | 178.5 | 245.41 | 201.8 |
| 115.30 | 106.7 | 159.15 | 147.6 | 203.42 | 179.6 | 247.88 | 203.0 |
| 117.72 | 109.3 | 161.60 | 149.4 | 205.89 | 181.7 | 250.35 | 203.7 |
| 120.14 | 110.9 | 164.06 | 151.7 | 208.35 | 183.1 | | |
| 122.56 | 113.9 | 166.52 | 153.4 | 210.82 | 184.4 | | |
| 124.99 | 116.5 | 168.97 | 155.4 | 213.29 | 185.7 | | |

## 2. Experimental

Adiabatic calorimetry was used to measure the heat capacity on powders in the temperature range (3 to 400) K. The calorimeter CAL V (Utrecht University) and its calibration were described previously [29]. Samples were prepared by co-precipitation from a solution of zirconium oxi-chloride $ZrOCl_2 \cdot 8H_2O$ and lanthanide nitrate $Ln(NO_3)_3 \cdot xH_2O$ with the right concentration using ammonia buffered to pH 11. Powders were sintered in air: 72 h at $T = 1723$ K for $Gd_2Zr_2O_7$, and 8 h at $T = 1773$ K for $Eu_2Zr_2O_7$. X-ray diffraction revealed only pyrochlore phases with lattice parameters of (1.051 and 1.057) nm, respectively. Specimens with weight of 17.1 g for $Gd_2Zr_2O_7$ and 11.2 g for $Eu_2Zr_2O_7$ were used. The experimental results are summarised in tables 1 and 2.

The heat capacity was also measured by an hybrid adiabatic relaxation method using a PPMS instrument (Quantum Design) on polycrystalline sample (pellet piece) in the temperature range (0.36 to 29) K. The accuracy of the PPMS instrument was verified by measuring a gold standard. The PPMS software used the two-tau relaxation method to determine the heat capacity values. $Gd_2Zr_2O_7$ pellets were obtained by pressing beads that were prepared by sol–gel method and subsequently calcined. The pellets were sintered in air for 72 h at $T = 1723$ K. $Eu_2Zr_2O_7$ pellets were obtained by pressing co-precipitated powder after

TABLE 2
Experimental heat capacity $C^{\circ}_{p,m}$ data for $Eu_2Zr_2O_7$ obtained with the adiabatic calorimeter at temperature $T$

| $T$/K | $C^{\circ}_{p,m}$ | $T$/K | $C^{\circ}_{p,m}$ | $T$/K | $C^{\circ}_{p,m}$ | $T$/K | $C^{\circ}_{p,m}$ |
|---|---|---|---|---|---|---|---|
| | $(J \cdot K^{-1} \cdot mol^{-1})$ | | $(J \cdot K^{-1} \cdot mol^{-1})$ | | $(J \cdot K^{-1} \cdot mol^{-1})$ | | $(J \cdot K^{-1} \cdot mol^{-1})$ |
| | | | | *Run 1* | | | |
| 296.77 | 234.2 | 322.71 | 242.5 | 349.52 | 249.8 | 376.44 | 256.4 |
| 298.86 | 235.4 | 325.68 | 243.3 | 352.51 | 250.5 | 379.44 | 257.1 |
| 301.85 | 236.2 | 328.66 | 244.2 | 355.49 | 251.3 | 382.44 | 257.9 |
| 304.83 | 237.1 | 331.64 | 244.8 | 358.48 | 252.2 | 385.45 | 258.5 |
| 307.81 | 238.1 | 334.62 | 245.7 | 361.47 | 252.8 | 388.45 | 259.3 |
| 310.79 | 239.0 | 337.60 | 246.6 | 364.46 | 253.4 | 391.46 | 259.8 |
| 313.77 | 239.7 | 340.58 | 247.4 | 367.45 | 254.3 | 394.47 | 260.4 |
| 316.75 | 240.5 | 343.56 | 248.0 | 370.44 | 255.0 | 397.48 | 260.9 |
| 319.73 | 241.4 | 346.54 | 249.0 | 373.44 | 255.7 | 400.50 | 261.5 |
| | | | | *Run 2* | | | |
| 6.21 | 0.125 | 14.77 | 1.21 | 20.77 | 4.20 | 27.57 | 9.32 |
| 9.55 | 0.275 | 15.90 | 1.34 | 22.11 | 5.03 | 28.93 | 10.85 |
| 11.31 | 0.422 | 17.07 | 2.01 | 23.45 | 6.06 | | |
| 12.64 | 0.611 | 18.30 | 2.78 | 24.79 | 7.18 | | |
| 13.66 | 0.927 | 19.51 | 3.50 | 26.16 | 8.72 | | |
| | | | | *Run 3* | | | |
| 5.72 | 0.213 | 11.76 | 0.597 | 16.59 | 2.01 | 21.59 | 4.63 |
| 7.23 | 0.151 | 13.58 | 1.03 | 18.23 | 2.65 | 23.34 | 5.89 |
| 9.16 | 0.249 | 15.08 | 1.43 | 19.90 | 3.67 | 25.15 | 7.66 |
| | | | | *Run 4* | | | |
| 28.09 | 10.36 | 44.74 | 29.19 | 64.09 | 55.21 | 84.86 | 82.78 |
| 29.66 | 11.71 | 46.78 | 31.88 | 66.34 | 58.22 | 87.22 | 85.79 |
| 31.42 | 13.49 | 48.86 | 34.70 | 68.62 | 61.34 | 89.59 | 88.77 |
| 33.19 | 15.44 | 50.97 | 37.42 | 70.90 | 64.43 | 91.96 | 91.74 |
| 34.98 | 17.42 | 53.10 | 40.28 | 73.20 | 67.49 | 94.34 | 94.65 |
| 36.84 | 19.72 | 55.25 | 43.15 | 75.51 | 70.56 | 96.73 | 97.58 |
| 38.76 | 21.63 | 57.43 | 46.15 | 77.84 | 73.59 | 99.12 | 100.5 |
| 40.73 | 24.05 | 59.63 | 49.18 | 80.17 | 76.66 | | |
| 42.72 | 26.66 | 61.85 | 52.17 | 82.51 | 79.73 | | |
| | | | | *Run 5* | | | |
| 98.55 | 99.47 | 124.07 | 128.9 | 150.96 | 154.7 | 178.01 | 176.7 |
| 99.88 | 101.4 | 126.50 | 131.3 | 153.42 | 156.9 | 180.47 | 178.5 |
| 102.32 | 104.7 | 128.94 | 133.9 | 155.88 | 159.0 | 182.93 | 180.3 |
| 104.73 | 107.3 | 131.38 | 136.4 | 158.33 | 161.1 | 185.40 | 182.1 |
| 107.13 | 110.5 | 133.82 | 138.8 | 160.79 | 163.1 | 187.86 | 183.9 |
| 109.54 | 113.3 | 136.26 | 141.1 | 163.26 | 165.1 | 190.32 | 185.6 |
| 111.95 | 115.8 | 138.71 | 143.5 | 165.71 | 167.2 | 192.79 | 187.4 |
| 114.37 | 118.4 | 141.16 | 145.8 | 168.17 | 169.2 | 195.26 | 189.0 |
| 116.79 | 121.0 | 143.61 | 148.0 | 170.63 | 171.1 | 197.72 | 190.6 |
| 119.21 | 123.4 | 146.06 | 150.3 | 173.09 | 172.9 | | |
| 121.64 | 125.7 | 148.51 | 152.6 | 175.55 | 174.8 | | |
| | | | | *Run 6* | | | |
| 197.47 | 190.2 | 229.62 | 207.8 | 261.88 | 221.9 | 294.25 | 234.0 |
| 199.92 | 191.7 | 232.10 | 209.0 | 264.37 | 222.9 | 296.75 | 234.9 |
| 202.41 | 193.3 | 234.58 | 210.2 | 266.86 | 224.0 | 299.25 | 235.6 |
| 204.87 | 194.9 | 237.06 | 211.5 | 269.34 | 224.9 | 301.75 | 236.3 |
| 209.81 | 197.4 | 242.02 | 213.7 | 274.32 | 226.9 | 306.74 | 238.2 |
| 212.29 | 198.8 | 244.50 | 214.9 | 276.80 | 227.7 | 309.23 | 239.0 |
| 214.76 | 200.2 | 246.98 | 216.0 | 279.29 | 228.6 | 311.73 | 239.6 |
| 217.24 | 201.5 | 249.46 | 217.0 | 281.78 | 229.5 | 314.23 | 240.4 |
| 219.71 | 202.8 | 251.94 | 218.3 | 284.28 | 230.5 | 316.73 | 241.1 |
| 222.19 | 204.0 | 254.43 | 218.6 | 286.77 | 231.3 | 319.23 | 241.8 |
| 224.67 | 205.3 | 256.91 | 219.7 | 289.26 | 231.5 | | |
| 227.15 | 206.5 | 259.40 | 220.8 | 291.76 | 233.1 | | |
| | | | | *Run 7* | | | |
| 299.12 | 235.8 | 326.45 | 244.1 | 353.73 | 251.7 | 381.10 | 258.6 |
| 301.64 | 236.7 | 328.93 | 244.8 | 356.21 | 252.3 | 383.59 | 259.2 |

TABLE 2 (*continued*)

| $T$/K | $C^{\circ}_{p,m}$ ($J \cdot K^{-1} \cdot mol^{-1}$) | $T$/K | $C^{\circ}_{p,m}$ ($J \cdot K^{-1} \cdot mol^{-1}$) | $T$/K | $C^{\circ}_{p,m}$ ($J \cdot K^{-1} \cdot mol^{-1}$) | $T$/K | $C^{\circ}_{p,m}$ ($J \cdot K^{-1} \cdot mol^{-1}$) |
|---|---|---|---|---|---|---|---|
| 304.12 | 237.3 | 331.41 | 245.6 | 358.70 | 253.0 | 386.09 | 259.7 |
| 306.61 | 238.1 | 333.89 | 246.3 | 361.18 | 253.7 | 388.59 | 260.3 |
| 309.10 | 239.0 | 336.37 | 247.0 | 363.66 | 254.2 | 391.09 | 260.5 |
| 311.58 | 239.5 | 338.85 | 247.7 | 366.15 | 254.9 | 393.59 | 261.2 |
| 314.06 | 240.4 | 341.33 | 248.3 | 368.64 | 255.5 | 396.09 | 262.5 |
| 316.54 | 240.9 | 343.81 | 249.0 | 371.13 | 256.1 | 398.60 | 263.0 |
| 319.02 | 241.6 | 346.29 | 249.8 | 373.62 | 256.7 | 401.11 | 262.9 |
| 321.50 | 242.6 | 348.77 | 250.4 | 376.11 | 257.3 | | |
| 323.97 | 243.4 | 351.25 | 251.0 | 378.61 | 257.9 | | |

compaction/milling steps and sintering in air for 2 h at $T = (1773$ and $1473)$ K. Pyrochlore phases were observed and lattice parameters of (1.055 and 1.0574) nm were measured for $Gd_2Zr_2O_7$ and $Eu_2Zr_2O_7$, respectively. The experimental data from the PPMS measurements are summarised elsewhere [27] and are available upon request from the authors.

## 3. Results and discussion

### 3.1. Gadolinium zirconate

The heat capacity of $Gd_2Zr_2O_7$ obtained by adiabatic calorimeter and PPMS measurements is plotted in figure 1, where the inset of the figure shows the results below $T = 25$ K. It exhibits a thermal anomaly below $T = 15$ K, which is related to the degeneracy of the ground state of the $Gd^{3+}$ ion (see below). At low temperature but above the thermal anomaly temperature domain, the heat capacity has been fitted to the equation $C_p = \alpha \cdot T^3$ (figure 2), yielding $C^{\circ}_p(Gd_2Zr_2O_7) = 4.952 \cdot 10^{-4} \cdot T^3$.

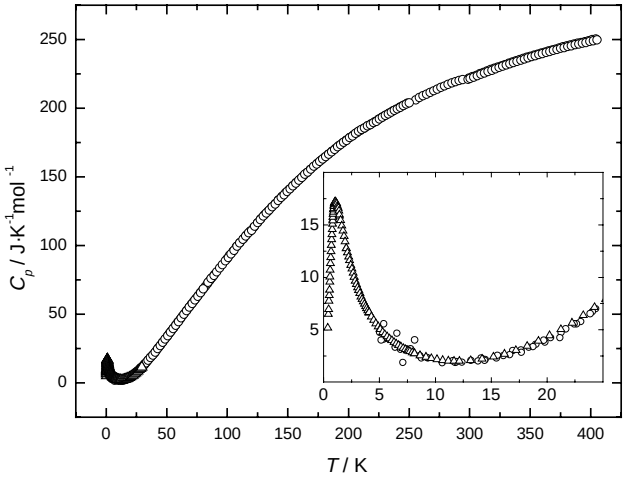


FIGURE 1. Heat capacity of $Gd_2Zr_2O_7$ measured by adiabatic calorimetry (○) and PPMS (△) plotted against temperature. The inset shows the low temperature measurements $T = (0$ to $25)$ K.

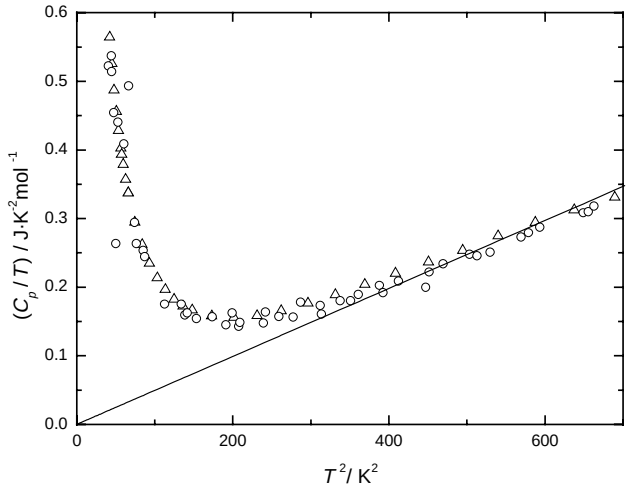


FIGURE 2. Low temperature heat capacity as $(C_p/T)$ of $Gd_2Zr_2O_7$ measured by adiabatic calorimetry (○) and PPMS (△) plotted against $T^2$; the solid line shows the $\alpha \cdot T^3$ fit as given in the text.

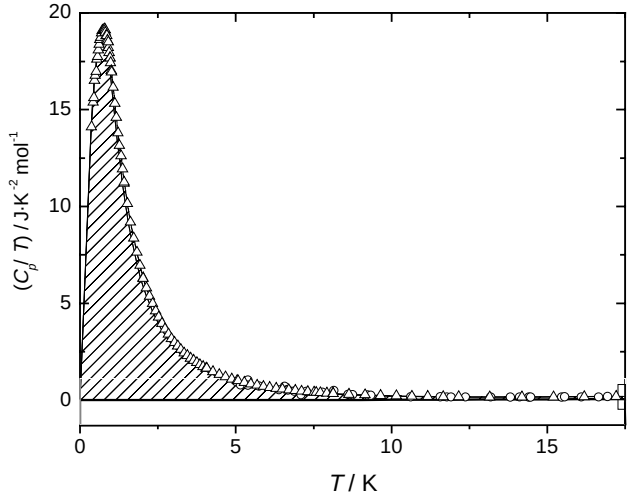


FIGURE 3. Low temperature heat capacity as $(C_p/T)$ of $Gd_2Zr_2O_7$ (—) measured by adiabatic calorimetry (○) and PPMS (△) and its lattice component (▬) plotted against temperature. The dashed area corresponds to the Schottky component.

From this equation, the heat capacity value at $T = 20$ K was obtained as $C_p^\circ(Gd_2Zr_2O_7, 20\ K) = 3.962\ J \cdot K^{-1} \cdot mol^{-1}$.

The heat capacity $C_p$ as well as the entropy $S$ can be described as the sum of two components: the lattice contribution $C_{lat}$ or $S_{lat}$ due to the vibrations of the ions in the crystal and the excess or Schottky contribution $C_{exs}$ or $S_{exs}$ due to the electron population of the Stark levels, arising from splitting of the ground state due to the crystal field. In case of $Gd_2Zr_2O_7$, in which the Gd ion has a half-filled 4f-shell, there is no crystal-field effect since the orbital part of the angular momentum is zero (spectroscopic term $^8S_{7/2}$). As a result the heat capacity measured corresponds to the lattice component, except in the temperature domain of the observed thermal anomaly (below $T = 15$ K). Thus, in the low temperature domain, extrapolation of equation (1) to $T = 0$ K yields the lattice contribution to the heat capacity, giving $S_{lat}(Gd_2Zr_2O_7, 20\ K) = 1.321\ J \cdot K^{-1} \cdot mol^{-1}$ by integration of $C_p/T$ from $T = (0$ to $20)$ K.

From the difference between the experimental curve (triangles in figure 3) and the lattice component determined (thick solid line in figure 3), the entropy change of the anomaly is obtained as $S_{exs}(Gd_2Zr_2O_7) = 35.430\ J \cdot K^{-1} \cdot mol^{-1} = 1.025 \cdot (2R \cdot \ln 8)$. This value is in excellent agreement with the theoretical value for a Schottky contribution arising from the ground-state degeneracy only, which is $R \cdot \ln(g_0)$ per mole of gadolinium. Since

TABLE 3
Smoothed thermodynamic functions of $Gd_2Zr_2O_7$ between $T = (20$ and $400)$ K ($\Phi_m^\circ(T) = -[\Delta G_m^\circ(T) - \Delta H_m^\circ(0\ K)]/T$)

| $T$/K | $C_{p,m}^0(T)$ | $S_m^\circ(T)$ | $\Delta_0^T H_m(T)$ | $\Phi_m^\circ(T)$ |
|---|---|---|---|---|
| | $(J \cdot K^{-1} \cdot mol^{-1})$ | $(J \cdot K^{-1} \cdot mol^{-1})$ | $(J \cdot mol^{-1})$ | $(J \cdot K^{-1} \cdot mol^{-1})$ |
| 20 | 3.962 | 36.75 | 88.72 | 32.3 |
| 25 | 7.500 | 37.97 | 116.5 | 33.3 |
| 30 | 11.48 | 39.67 | 165.6 | 34.2 |
| 35 | 16.64 | 41.82 | 235.5 | 35.1 |
| 40 | 21.62 | 44.37 | 331.1 | 36.1 |
| 45 | 27.37 | 47.25 | 453.8 | 37.2 |
| 50 | 33.19 | 50.43 | 604.9 | 38.3 |
| 55 | 39.02 | 53.87 | 786.1 | 39.6 |
| 60 | 44.79 | 57.51 | 995.8 | 40.9 |
| 65 | 50.69 | 61.33 | 1234 | 42.4 |
| 70 | 56.46 | 65.30 | 1502 | 43.8 |
| 75 | 62.20 | 69.39 | 1799 | 45.4 |
| 80 | 67.98 | 73.59 | 1617 | 47.0 |
| 85 | 73.77 | 77.88 | 2477 | 48.7 |
| 90 | 79.30 | 82.25 | 2859 | 50.5 |
| 95 | 84.79 | 86.68 | 3271 | 52.3 |
| 100 | 90.19 | 91.17 | 3708 | 54.1 |
| 110 | 101.3 | 100.3 | 4662 | 57.9 |
| 120 | 110.8 | 109.6 | 5731 | 61.8 |
| 130 | 121.5 | 118.9 | 6894 | 65.8 |
| 140 | 130.5 | 128.2 | 8149 | 70.0 |
| 150 | 139.9 | 137.5 | 9510 | 74.1 |
| 160 | 148.3 | 146.8 | 10,958 | 78.3 |
| 170 | 156.3 | 156.1 | 12,457 | 82.8 |
| 180 | 163.9 | 165.2 | 14,081 | 87.0 |
| 190 | 171.1 | 174.3 | 15,754 | 91.3 |
| 200 | 177.8 | 183.2 | 17,471 | 95.9 |
| 210 | 183.8 | 192.0 | 19,311 | 100.1 |
| 220 | 189.1 | 200.7 | 21,166 | 104.5 |
| 230 | 194.3 | 209.2 | 23,064 | 108.9 |
| 240 | 199.4 | 217.6 | 25,059 | 113.2 |
| 250 | 203.6 | 225.8 | 27,064 | 117.6 |
| 260 | 208.2 | 233.9 | 29,120 | 121.9 |
| 270 | 212.4 | 241.8 | 31,223 | 126.2 |
| 280 | 215.8 | 249.6 | 33,367 | 130.5 |
| 290 | 219.2 | 257.3 | 35,548 | 134.7 |
| 298.15 | 221.8 | 263.4 | 37,346 | 138.1 |
| 300 | 222.4 | 264.8 | 37,755 | 138.9 |
| 310 | 225.4 | 272.1 | 39,985 | 143.1 |
| 320 | 228.1 | 279.3 | 42,250 | 147.3 |
| 330 | 231.3 | 286.4 | 44,548 | 151.4 |
| 340 | 234.2 | 293.3 | 46,875 | 155.4 |
| 350 | 237.0 | 300.1 | 49,231 | 159.5 |
| 360 | 239.7 | 306.9 | 51,615 | 163.5 |
| 370 | 242.2 | 313.5 | 54,024 | 167.4 |
| 380 | 244.6 | 320.0 | 56,458 | 171.4 |
| 390 | 246.7 | 326.3 | 58,915 | 175.3 |

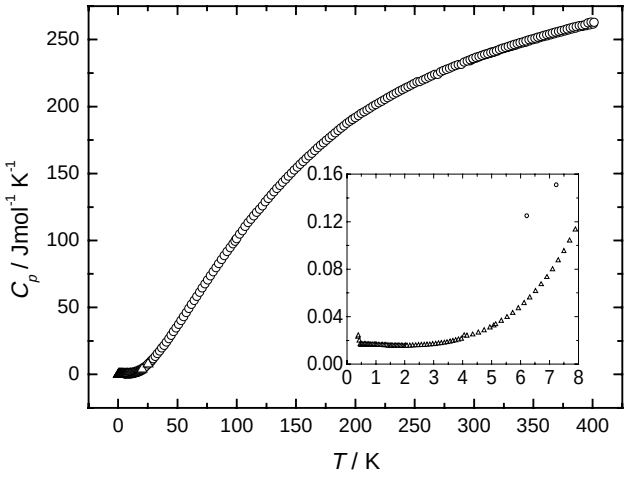


FIGURE 4. Heat capacity of $Eu_2Zr_2O_7$ measured by adiabatic calorimetry (○) and PPMS (△) plotted against temperature. The inset shows the low temperature measurements $T = (0$ to $8)$ K.

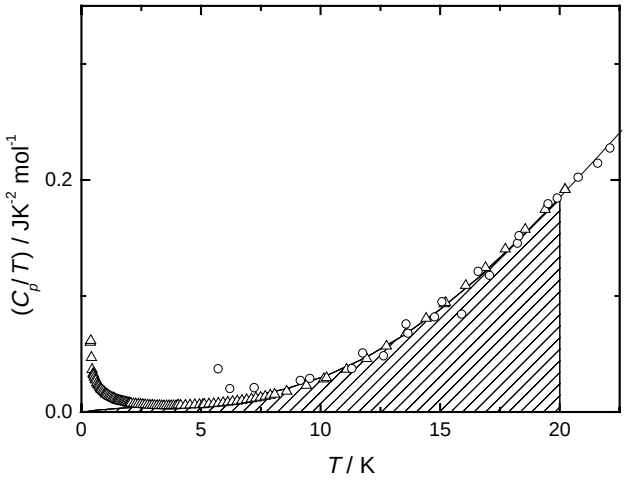


FIGURE 5. Low temperature heat capacity as $(C_p/T)$ of $Eu_2Zr_2O_7$ measured by adiabatic calorimetry (○) and PPMS (△) plotted against temperature, and the interpolation to $T = 0$ K. The dashed area corresponds to the entropy at $T = 20$ K.

the ground multiplet is $^8S_{7/2}$, the degeneracy is $g_0 = 8$. The total entropy can then be obtained from the sum of the lattice and the Schottky component, yielding $S^\circ(Gd_2Zr_2O_7, 20\ K) = 36.751\ J \cdot K^{-1} \cdot mol^{-1}$. Using the heat capacity and the entropy at $T = 20$ K, the smoothed thermodynamic functions of $Gd_2Zr_2O_7$ were derived in the temperature range (20 to 400) K and are summarised in table 3.

### 3.2. Europium zirconate

The heat capacity data obtained for $Eu_2Zr_2O_7$ by adiabatic calorimeter and PPMS measurements are plotted in figure 4 where the inset of the figure shows the low temperature results (below $T = 8$ K). Below $T = 8$ K, the adiabatic data are scattered, which is due to the fact that the apparatus was operated at its lower temperature limit.

No thermal anomaly is expected for this compound as the ground term is $^7F_0$ and its degeneracy $g_0 = 1$. However, a small anomalous tendency is visible below $T = 1$ K. This could be due to the presence of $Gd^{3+}$ or $Eu^{2+}$ impurity ($g_0 = 8$). The analysis report of the europium nitrate precursor mentioned $10 \cdot 10^{-6}$ gadolinium impurity and, as the compound was sintered in air, $Eu^{2+}$ is not expected. Since the thermal anomaly observed for $Gd^{3+}$ is so intense that even a small quantity of $Gd^{3+}$ would be detected, the anomalous behaviour in $Eu_2Zr_2O_7$ is assigned to this impurity and will be neglected for the further analysis.

From data measured in the temperature range (3 to 20) K the heat capacity of $Eu_2Zr_2O_7$ has been extrapolated to $T = 0$ K, as shown in figure 5. From this curve, the heat capacity has been determined at $T = 20$ K, yielding $C_p^\circ(Eu_2Zr_2O_7, 20\ K) = 3.697\ J \cdot K^{-1} \cdot mol^{-1}$. The entropy at the same temperature has been determined as the surface under the curve between $T = (0$ and $20)$ K, as shown by the dashed surface in figure 5, yielding $S^\circ(Eu_2Zr_2O_7, 20\ K) = 1.055\ J \cdot K^{-1} \cdot mol^{-1}$. Using the heat capacity and the entropy at $T = 20$ K, the thermodynamic functions of $Eu_2Zr_2O_7$ were derived in the temperature range (20 to 400) K and are summarised in table 4.

TABLE 4
Smoothed thermodynamic functions of $Eu_2Zr_2O_7$ between $T = (20$ and $400)$ K ($\Phi_m^\circ(T) = -[\Delta G_m^\circ(T) - \Delta H_m^\circ(0\ K)]/T$)

| $T$/K | $C_{p,m}^0(T)$ | $S_m^\circ(T)$ | $\Delta_0^T H_m(T)$ | $\Phi_m^\circ(T)$ |
|---|---|---|---|---|
| | $(J \cdot K^{-1} \cdot mol^{-1})$ | $(J \cdot K^{-1} \cdot mol^{-1})$ | $(J \cdot mol^{-1})$ | $(J \cdot K^{-1} \cdot mol^{-1})$ |
| 20 | 3.697 | 1.055 | 15.98 | 0.256 |
| 25 | 7.462 | 2.050 | 42.81 | 0.337 |
| 30 | 12.05 | 3.813 | 92.05 | 0.744 |
| 35 | 17.44 | 6.068 | 165.2 | 1.349 |
| 40 | 23.12 | 8.773 | 267.0 | 2.099 |
| 45 | 29.53 | 11.87 | 398.7 | 3.009 |
| 50 | 36.16 | 15.32 | 563.0 | 4.064 |
| 55 | 42.81 | 19.08 | 760.5 | 5.255 |
| 60 | 49.68 | 23.10 | 992 | 6.572 |
| 65 | 56.43 | 27.34 | 1257 | 8.006 |
| 70 | 63.22 | 31.77 | 1556 | 9.544 |
| 75 | 69.88 | 36.36 | 1889 | 11.18 |
| 80 | 76.44 | 41.08 | 2255 | 12.90 |
| 85 | 82.96 | 45.91 | 2653 | 14.70 |
| 90 | 89.28 | 50.83 | 3084 | 16.57 |
| 95 | 95.46 | 55.83 | 3546 | 18.50 |
| 100 | 101.5 | 60.88 | 4041 | 20.47 |
| 110 | 113.8 | 71.14 | 5118 | 24.61 |
| 120 | 124.1 | 81.49 | 6309 | 28.92 |
| 130 | 135.0 | 91.86 | 7605 | 33.36 |
| 140 | 144.7 | 102.2 | 9004 | 37.91 |
| 150 | 153.9 | 112.5 | 10,497 | 42.55 |
| 160 | 162.4 | 122.7 | 12,079 | 47.24 |
| 170 | 170.7 | 132.8 | 13,745 | 51.98 |
| 180 | 178.2 | 142.8 | 15,489 | 56.75 |
| 190 | 185.4 | 152.6 | 17,307 | 61.54 |
| 200 | 191.8 | 162.3 | 19,194 | 66.33 |
| 210 | 197.5 | 171.8 | 21,142 | 71.13 |
| 220 | 202.9 | 181.1 | 23,145 | 75.92 |
| 230 | 208.0 | 190.3 | 25,199 | 80.69 |
| 240 | 212.8 | 199.2 | 27,303 | 85.45 |
| 250 | 217.3 | 208.0 | 29,454 | 90.17 |
| 260 | 221.1 | 216.6 | 31,645 | 94.87 |
| 270 | 225.2 | 225.0 | 33,877 | 99.54 |
| 280 | 228.9 | 233.3 | 36,147 | 104.2 |
| 290 | 231.9 | 241.4 | 38,453 | 108.8 |
| 298.15 | 235.4 | 247.8 | 40,359 | 112.5 |
| 300 | 235.7 | 249.3 | 40,794 | 113.3 |
| 310 | 239.0 | 257.1 | 43,168 | 117.8 |
| 320 | 242.1 | 264.7 | 45,576 | 122.3 |
| 330 | 245.2 | 272.2 | 48,013 | 126.7 |
| 340 | 248.0 | 279.6 | 50,479 | 131.1 |
| 350 | 250.7 | 286.8 | 52,973 | 135.5 |
| 360 | 253.4 | 293.9 | 55,493 | 139.8 |
| 370 | 255.8 | 300.9 | 58,038 | 144.0 |
| 380 | 258.3 | 307.7 | 60,609 | 148.2 |
| 390 | 260.4 | 314.5 | 63,203 | 152.4 |

## 4. Discussion

The heat capacity of $Gd_2Zr_2O_7$ and $Eu_2Zr_2O_7$ are compared in figure 6 to the results previously obtained for $Nd_2Zr_2O_7$ by the present authors [28] and for

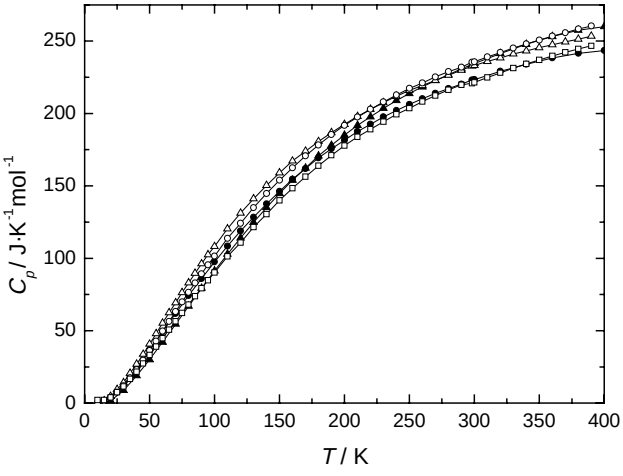


FIGURE 6. Heat capacity obtained for $Gd_2Zr_2O_7$ (□) and $Eu_2Zr_2O_7$ (○) plotted against temperature compared to the results reported for $Nd_2Zr_2O_7$ (△) by the present authors [28] and for $La_2Zr_2O_7$ (●) and $Ce_2Zr_2O_7$ (▲) by Bolech *et al.* [24,25].

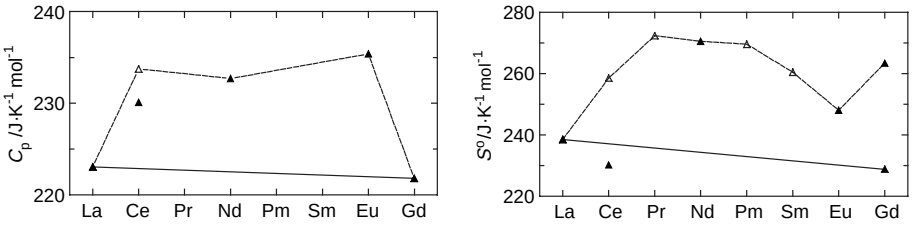


FIGURE 7. Heat capacity and entropy of the lanthanide zirconate $Ln_2Zr_2O_7$ for Ln = La to Gd at the standard temperature $T = 298.15$ K. Closed symbols (▲) indicate the measured values, and the lattice component interpolated from the $La_2Zr_2O_7$ and $Gd_2Zr_2O_7$ values is shown as a solid line. The open symbols (△) show the values estimated from the ground-state degeneracy (see detail in Section 4), except for $Ce_2Zr_2O_7$ which have been calculated from the crystal field energies.

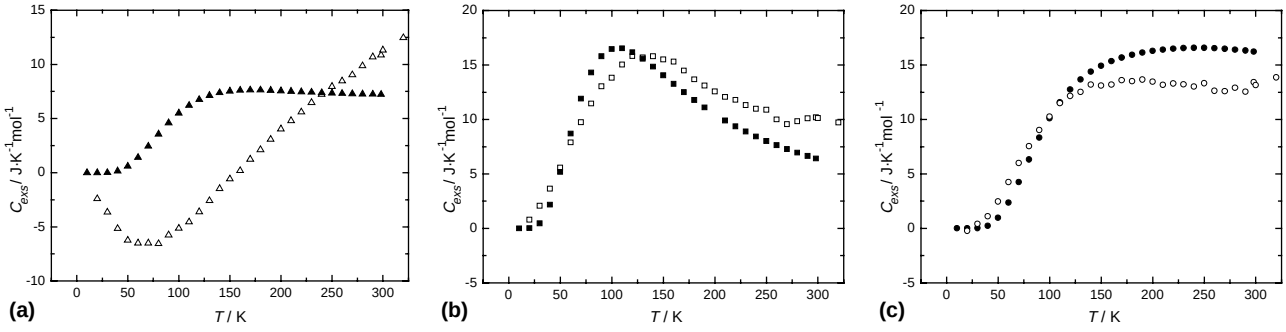


FIGURE 8. The excess (Schottky) heat capacity of: (a) $Ce_2Zr_2O_7$ (△), (b) $Nd_2Zr_2O_7$ (□) and (c) $Eu_2Zr_2O_7$ (○). Open symbols correspond to the experimental values and closed symbols to values calculated from the energy level according to equation (1).

$La_2Zr_2O_7$ and $Ce_2Zr_2O_7$ by Bolech *et al.* [24,25]. The heat capacity curves of $La_2Zr_2O_7$ and $Gd_2Zr_2O_7$ are almost identical above $T = 20$ K. The curves of $Eu_2Zr_2O_7$ and $Nd_2Zr_2O_7$ have the same shape but are slightly different, whereas the curve of $Ce_2Zr_2O_7$ is the lowest at low temperature and the highest at high temperature. On first sight these differences can be explained by the effect of the Schottky contribution.

The excess or Schottky contribution can be calculated from the crystal field energies according to the following equations where $Q$ is the partitioning function described by the Maxwell–Boltzmann distribution law in equation (3), $T$ the temperature, $R$ the universal gas constant, $E_i$ the energy of the level $i$, and $g_i$, its degeneracy

$$C_{\text{exs}} = Q^{-2}\cdot R^{-2}\cdot T^{-2}\cdot\left[Q\cdot\sum_{i=1}^{n} g_i\cdot E_i^2\cdot\exp(-E_i/R\cdot T) - \left\{\sum_{i=1}^{n} g_i\cdot E_i\cdot\exp(-E_i/R\cdot T)\right\}^2\right], \quad (1)$$

$$S_{\text{exs}} = R\cdot\ln(g_o) + R\cdot\ln\left\{\sum_{i=1}^{n} g_i\cdot\exp(-E_i/R\cdot T)\right\}, \quad (2)$$

$$Q = \sum_{i=0}^{n} g_i\cdot\exp(-E_i/R\cdot T). \quad (3)$$

TABLE 5
Energy levels of the $Ln^{3+}$ cations in the pyrochlore structure $Ln_2Zr_2O_7$

| | [SL]J-state | Degeneracy | Energy[a] $(hc)^{-1}$/cm$^{-1}$ |
|---|---|---|---|
| $Ce_2Zr_2O_7$ | $^2F_{5/2}$ | 2 | 0 |
| | | 2 | 253 |
| | | 2 | 875 |
| | $^2F_{7/2}$ | 2 | 2123 |
| | | 2 | 2630 |
| | | 2 | 2716 |
| | | 2 | 3659 |
| $Nd_2Zr_2O_7$ | $^4I_{9/2}$ | 2 | 0 |
| | | 2 | 164 |
| | | 2 | 224 |
| | | 2 | 234 |
| | | 2 | 590 |
| | $^4I_{11/2}$ | 2 | 1900 |
| | | 2 | 2027 |
| | | 2 | 2052 |
| | | 2 | 2085 |
| | | 2 | 2251 |
| | | 2 | 2263 |
| $Eu_2Zr_2O_7$ | $^7F_0$ | 1 | 0 |
| | $^7F_1$ | 2 | 264 |
| | | 1 | 612 |
| | $^7F_2$ | 2 | 762 |
| | | 1 | 880 |
| | | 2 | 1452 |
| | $^7F_3$ | 1 | 1714 |
| | | 1 | 1776 |
| | | 2 | 1965 |
| | | 2 | 2145 |
| | | 1 | 2236 |

[a] $h$ is Planck constant and $c$ is the speed of light in vacuum.

In general, the lattice heat capacity of isostructural lanthanide compounds are close to each other and linearly decrease along the series [30]. In the temperature range between $T = (20$ and $300)$ K the Schottky contributions to the heat capacity are zero for the La and Gd compounds as their lanthanide f-shell are empty and half-filled, respectively. The excess contribution to the entropy is also zero for $La_2Zr_2O_7$ and is only composed of the ground level contribution for $Gd_2Zr_2O_7$. From these statements, the lattice component of the heat capacity and of the entropy can be interpolated from the $La_2Zr_2O_7$ and $Gd_2Zr_2O_7$ values for the complete lanthanide series (with the value $2R \cdot \ln 8$ subtracted from the $Gd_2Zr_2O_7$ entropy data). These interpolations are shown for $T = 298.15$ K in figure 7 and have been reproduced for the complete temperature range (20 to 400) K.

By subtracting these lattice heat capacity values from the measured data, the Schottky heat capacity has been determined. The resulting values are plotted as open symbols in figure 8. The excess contribution to the heat capacity of $Ce_2Zr_2O_7$ is negative between $T = (20$ and $150)$ K which is not in agreement with the expected behaviour. The significantly lower heat capacity of $Ce_2Zr_2O_7$ compared to $La_2Zr_2O_7$ was explained by Bolech as the result of lattice defects introduced by the sintering. However, it can also be an effect of a partial oxidation of the cerium into $Ce^{4+}$.

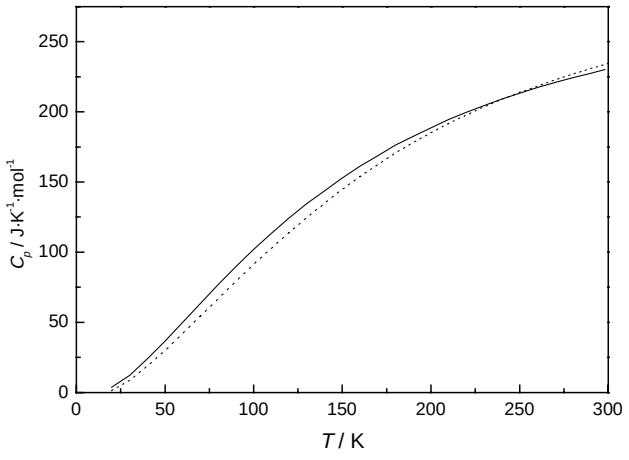


FIGURE 9. Calculated (—) and experimental (···) [24,25] heat capacity of $Ce_2Zr_2O_7$ plotted against the temperature.

The Schottky contributions of the zirconates have also been calculated from the crystal field energies of the lanthanide ions in the pyrochlore structure. The electronic energy levels were obtained from optical spectroscopy measurements on $La_2Zr_2O_7$ doped with 5% Eu, scaled using the crystal field parameters of $Ho_2Ti_2O_7$ [31]. The resulting energy levels are summarised in table 5. The Schottky contributions to the heat capacity thus obtained are plotted as closed symbols in figure 8. Except for $Ce_2Zr_2O_7$ these data agree well with those determined from the experimental heat capacity data. The shapes of the experimental and calculated curves are similar, but do not fully overlap, indicating that the crystal field energies need further refining.

The total heat capacity of $Ce_2Zr_2O_7$ has been simulated from the lattice components determined by interpolation and from the Schottky contributions calculated from the crystal field energies. The results are plotted in figure 9. Table 6 gives the resulting entropy value at $T = 298.15$ K, which is 28.3 $J \cdot K^{-1} \cdot mol^{-1}$ higher than the result of Bolech *et al.* [24,25]. In this table, the entropies of the other lanthanide pyrochlore zirconates are estimated, from the lattice component and the excess contribution calculated from the degeneracy of the lowest [SL]J-state, neglecting crystal field splitting. This may lead to a small overestimation of the entropies of up to 4 $J \cdot K^{-1} \cdot mol^{-1}$.

TABLE 6
The standard entropies (at $T = 298.15$ K) of the lanthanide pyrochlores $Ln_2Zr_2O_7$ obtained from the lattice and excess components ($S_{tot} = S_{lat} + 2S_{exs}$)

| | $S_{lat}$ | $S_{exs}$ | $S_{tot}$ | $S_{exp}$ |
|---|---|---|---|---|
| | ($J \cdot K^{-1} \cdot mol^{-1}$) | ($J \cdot K^{-1} \cdot mol^{-1}$) | ($J \cdot K^{-1} \cdot mol^{-1}$) | ($J \cdot K^{-1} \cdot mol^{-1}$) |
| $La_2Zr_2O_7$ | 238.5 | 0.00 | 238.5 | $238.5 \pm 0.5$[a] |
| $Ce_2Zr_2O_7$ | 237.1 | 10.69 | 258.5 | $230.2 \pm 0.5$[a] |
| $Pr_2Zr_2O_7$ | 235.8 | *18.27* | *272.3* | |
| $Nd_2Zr_2O_7$ | 234.4 | 17.13 | 268.6 | $270.5 \pm 0.6$[b] |
| $Pm_2Zr_2O_7$ | 233.0 | *18.27* | *269.5* | |
| $Sm_2Zr_2O_7$ | 231.6 | *14.42* | *260.4* | |
| $Eu_2Zr_2O_7$ | 230.2 | 9.92 | 250.01 | $247.8 \pm 0.5$[c] |
| $Gd_2Zr_2O_7$ | 228.8 | 17.29 | 263.4 | $263.4 \pm 0.5$[c] |

When the excess values are given in italic numbers, the value has been obtained from the unsplit lowest [SL]J-state.

[a] Bolech *et al.* [24].

[b] Lutique *et al.* [28]; note that the correct value at $T = 298.15$ K is $S^\circ_m = (270.5 \pm 0.6)$ $J \cdot K^{-1} \cdot mol^{-1}$ as given in table 3 of [28] and not $(264.1 \pm 0.6)$ $J \cdot K^{-1} \cdot mol^{-1}$ as given in the text of this reference (which is the value at $T = 290$ K).

[c] This study.

## 5. Conclusions

The thermodynamic functions of $Gd_2Zr_2O_7$ and $Eu_2Zr_2O_7$ were determined in the temperature range (20 to 400) K from heat capacity measurements. Their heat capacity and entropy were compared with those of $Nd_2Zr_2O_7$, $La_2Zr_2O_7$ and $Ce_2Zr_2O_7$ available in the literature. From the results the lattice heat capacity was determined by interpolation between $La_2Zr_2O_7$ and $Gd_2Zr_2O_7$ and the Schottky contribution was determined by subtracting the lattice heat capacity from the experimental data. These data were compared with values calculated from crystal field energies. Except for $Ce_2Zr_2O_7$, both sets of data are coherent. The total heat capacity and entropy of this compound has been deduced for the other lanthanide pyrochlores from the calculated lattice and Schottky contributions.

## Acknowledgements

S.L. and P.J. acknowledge the European Commission for support given in the frame of the program "training and mobility of researchers".

## References

[1] A.P. Ramirez, A. Hayashi, R.J. Cava, R. Siddharthan, B.S. Shastry, Nature 399 (1999) 333–335.
[2] P. Bonville, J.A. Hodges, M. Ocio, J.P. Sanchez, P. Vulliet, S. Sosin, D. Braithwaite, J. Phys. Condens. Matter 15 (2003) 7777–7778.
[3] R. Higashinaka, H. Ukazawa, Y. Maeno, Physica B 329–333 (2003) 1040–1041.
[4] R. Vassen, X.Q. Cao, D. Basu, D. Stöver, J. Am. Ceram. Soc. 83 (2000) 2023–2028.
[5] J. Wu, X. Wei, N.P. Padture, P.G. Klemens, M. Gell, E. Garcia, P. Miranzo, M.I. Osendi, J. Am. Ceram. Soc. 85 (2002) 3031–3035.
[6] X.Q. Cao, R. Vassen, W. Jungen, S. Schwartz, F. Tietz, D. Stöver, J. Am. Ceram. Soc. 84 (2001) 2086–2090.
[7] N.P. Padture et al., Acta Mater. 49 (2001) 2251–2257.
[8] T. Omata, H. Kishimoto, S. Otsuka-Yao-Matsuo, N. Ohtori, N. Umesaki, J. Solid-State Chem. 147 (1999) 573–583.
[9] N. Izu, T. Omata, S. Otsuka-Yao-Matsuo, J. Alloys Comp. 270 (1998) 107–114.
[10] S. Otsuka-Yao-Matsuo, T. Omata, N. Izu, H. Kishimoto, J. Solid-State Chem. 138 (1998) 47–54.
[11] S. Otsuka-Yao-Matsuo, N. Izu, T. Omata, K. Ikeda, J. Electrochem. Soc. 145 (1998) 1406–1413.
[12] P.E. Raison, R.G. Haire, in: Proceeding GLOBAL'01, 9–13 Sept. 2001, Paris (on cd-rom).
[13] P.E. Raison, R.G. Haire, Z. Assefa, J. Nucl. Sci. Technol. (Suppl. 3) (2002) 725–728.
[14] S. Lutique, R.J.M. Konings, V.V. Rondinella, J. Somers, D. Staicu, T. Wiss, J. Nucl. Mater. 319 (2003) 59–64.
[15] S. Lutique, R.J.M. Konings, V.V. Rondinella, J. Somers, T. Wiss, in: CIMTEC 2002 – 10th International Ceramic Congress – Part D, 15–18 July 2002, Florence, Italy; Advances in Science and Technology, Vincenzini. P., pp. 241–248.
[16] S. Lutique, R.J.M. Konings, V.V. Rondinella, J. Somers, T. Wiss, J Alloys Comp. 352 (2003) 1–5.
[17] B.D. Begg, W.J. Weber, R. Devanathan, J.P. Icenhower, S. Thevuthasan, B. P. McGrail, Heavy-ion irradiation effects in pyrochlores, in: Environmental Issues and Waste Management Technologies V, 2000, pp. 553–560.
[18] B.D. Begg, N.J. Hess, W.J. Weber, R. Devanathan, J.P. Icenhower, S. Thevuthasan, B.P. McGrail, J. Nucl. Mater. 288 (2001) 208–216.
[19] S.X. Wang, B.D. Begg, L.M. Wang, R.C. Ewing, W.J. Weber, K.V. Godivan Kutty, J. Mater. Res. 14 (1999) 4470–4473.
[20] W.J. Weber, J.M. Wald, H. Matzke, Mater. Lett. 3 (1985) 173–180.
[21] J.M. Wald, P. Offermann, A study of radiation effects in curium-doped $Gd_2Ti_2O_7$ (pyrochlore) and $CaZrTi_2O_7$ (zirconolite), in: W. Lutze (Ed.), Scientific Basis for Radioactive Waste Management XII, 1982, pp. 369–378.
[22] V.R. Korneev, V.B. Glushkova, E.K. Keler, Izv. Akad. Nauk. SSSR Neorg. Materialy 7 (1971) 886–887.
[23] M. Bolech, E.H.P. Cordfunke, F.J.J.G. Janssen, A. Navrotsky, J. Am. Ceram. Soc. 78 (1995) 2257–2258.
[24] M. Bolech, E.H.P. Cordfunke, A.C.G. van Genderen, R.R. van der Laan, F.J.J.G. Janssen, J.C. Van Miltenburg, J. Phys. Chem. Solids 58 (1997) 433–439.
[25] M. Bolech, Ph.D. Thesis, University of Amsterdam, The Netherlands, 1998.
[26] K.B. Helean, B.D. Begg, A. Navrotsky, B. Ebbinghaus, W.J. Weber, R.C. Ewing, Mater. Res. Soc. Symp. Proc. 663 (2001) 691–697.
[27] S. Lutique, Ph.D. Thesis, Université de Paris-Sud, U.F.R. Scientifique d'Orsay, France, 2003.
[28] S. Lutique, P. Javorskỳ, R.J.M. Konings, J.C. van Miltenburg, A.C.G. van Genderen, F. Wastin, J. Chem. Thermodyn. 35 (2003) 955–965.
[29] J.C. van Miltenburg, G.J.K. van den Berg, M.J. van Bommel, J. Chem. Thermodyn. 19 (1987) 1129–1138.
[30] R.J.M. Konings, J. Nucl. Mater. 295 (2001) 57–63.
[31] S. Rosenkranz, A.P. Ramirez, A. Hayashi, R.J. Cava, R. Siddharthan, B.S. Shastry, J. Appl. Phys. 87 (2000) 5914–5916.

JCT 04/26